JOURNAL OF AIRCRAFT
Vol. 38, No. 1, January–February 2001

Displacement and Strain Statistics of Thermally Buckled Plates

Jon Lee*
U.S. Air Force Research Laboratory, Wright–Patterson Air Force Base, Ohio 45433

Previously, we used the single-mode Fokker–Planck distribution to predict displacement histograms of the numerical simulations and strain histograms of the plate experiments. Such an elemental distribution has proven effective in capturing the overall behavior of numerical displacement histograms. This is because the Fokker–Planck distribution is realizable. On the other hand, there are two possible equilibrium strain distributions derived from the Fokker–Planck distribution, one of which drops out when the forcing power input is small. By restricting the other strain distribution to a small forcing range, we have exhibited the skewing of experimental strain histograms toward the negative strain. We show here that the actual strain histograms of numerical simulation are neither one of the equilibrium strain distributions, but can be modeled by a linear combination of them. Hence, the unequal strain peaks may not be entirely due to a temperature gradient across the plate thickness, as previously proposed.

Nomenclature

C_0, C_1, C_2	=	coefficients for normal x strain
D	=	forcing power input
$f(q),\ f_\pm(\varepsilon)$	=	Fokker–Planck type distributions
f_0	=	$t_0\delta_g(\beta^4 + 2\beta^2/3 + 1)/6$
$g(t),\ \bar{g}(\tau)$	=	forcing time series
H	=	Hamiltonian
h	=	plate thickness
L_x, L_y	=	plate sides
$Q_\pm$	=	postbuckled plate displacements
q	=	transverse displacement
s	=	thermal buckling parameter
t, τ	=	times
t_0	=	uniform plate temperature
z	=	$\varpi^2(s-1)\sqrt{(2\nu/\alpha D)}$
α	=	cubic nonlinear coefficient
β	=	L_y/L_x
γ	=	time scaling factor
δ_v, δ_g	=	scaling factors for temperature variation and gradient
ε	=	normal x strain
μ	=	Poisson's ratio
ν	=	$2\varsigma\varpi$
Ξ	=	Young's modulus
ϖ	=	$\sqrt{[16(\beta^4 + 2\beta^2/3 + 1)/3]}$
ρ	=	mass density of plate
$\sigma, \sigma_r, \sigma_\varepsilon$	=	standard deviations
ς	=	damping coefficient

Introduction

FOR high performance military aircraft and future high-speed civil transport planes, certain structural skin components are subjected to very large acoustic loads in an elevated thermal environment.[1] Hence, the dual effect of thermal and acoustic loading has given rise to the so-called thermal-acoustic structural fatigue.[2,3] Generally, raising the plate temperature uniformly under immovable edge boundary constraints will result in thermal buckling, just as one observes flexural buckling as the in-plane stress along plate edges is increased beyond a certain critical value. This equivalence has been recognized[4,5] and exploited in the analytical and experimental investigations of thermal-acoustic structural fatigue.[6,7] Under the sound pressure level (SPL) of 140–160 dB in NASA's Thermal Acoustic Fatigue Apparatus, Ng and Clevenson[8] have achieved sufficient plate heating to observe the erratic snap-through under acoustic random excitations. Furthermore, Ng,[7] Ng and Clevenson,[8] and Ng and Wentz[9] observed that a single-mode model of plate equations could explain certain features of the plate experiments.

We have, therefore, initiated study of the single-mode model for a heated plate, written in a standard oscillator form for displacement q:

$$\ddot{q} + 2\varsigma\varpi\dot{q} + \varpi^2(1-s)q + \alpha q^3 = f_0 + g(t) \tag{1}$$

where the overdot denotes $\mathrm{d}/\mathrm{d}t$, ς is the damping ratio, and g represents the external forces. For a clamped plate, we have the following system parameters:

$$\varpi^2 = \tfrac{16}{3}(\beta^4 + 2\beta^2/3 + 1)$$

$$s = t_0\left(1 + \delta_v\left\{\frac{1}{4} + \frac{1}{6}(1-\mu)\left[1 + \frac{\beta^2}{(1+\beta^2)^2}\right]\right\}\right)$$

$$\alpha = \frac{32}{3}\left\{\beta^4 + 1 + 2\mu\beta^2 + \frac{4}{9}(1-\mu^2)\left[\frac{17}{8}(\beta^4+1) + \frac{4\beta^4}{(\beta^2+1)^2} + \frac{\beta^4}{(\beta^2+4)^2} + \frac{\beta^4}{(4\beta^2+1)^2}\right]\right\}$$

$$f_0 = (t_0\delta_g/6)(\beta^4 + 2\beta^2/3 + 1)$$

Here, $\beta = L_y/L_x$ is the aspect ratio of plate sides L_x and L_y. The uniform plate temperature t_0 is measured in units of the critical buckling temperature. Note that the expressions for s and f_0 are specific to the temperature variation and gradient distributions assumed in Ref. 1. That is, we let $(t_0\delta_v)\sin^2(\pi x)\sin^2(\pi y)$ be the temperature variation over the midplate and let $(t_0\delta_g)\sin^2(\pi x)\sin^2(\pi y)$ be the distribution of temperature gradient across the plate thickness. Here, the amplitudes $t_0\delta_v$ and $t_0\delta_g$ are given by the scaling factors δ_v and δ_g. Note that Eq. (1) is nondimensional. That is, q is measured in units of plate thickness h (inches), time t in units of $\gamma = \sqrt{[(1-\mu^2)\rho L_y^4/\pi^4 h^2 \Xi g_c]}$ (seconds), and $g(t)$ in units of $g_{\mathrm{psi}} = \rho h^2/12\gamma^2 g_c$ (pounds per square inch) (see Ref. 10). Here, $g_c = 32.2$ is the acceleration constant.

Suppose that the forcing has zero mean $\langle g(t)\rangle = 0$ and delta-correlation variance $\langle g(t)g(t')\rangle = 2D\delta(t-t')$, where $\langle\cdots\rangle$ denotes

Received 9 April 1999; presented as Paper 99-1457 at the AIAA/ASME/ASCE/AHS/ASC 40th Structures, Structural Dynamics, and Materials Conference, St. Louis, MO, 12–15 April 1999; revision received 24 November 1999; accepted for publication 11 December 1999.

*Research Scientist, Structural Dynamics Branch; jon.lee@wpafb.af.mil.

statistical average and D is constant power input. For a stationary statistical solution of Eq. (1), we have the Fokker–Planck distribution for displacement[11,12]:

$$f(q) = N \exp\left\{-(\nu/D)\left[\tfrac{1}{2}\varpi^2(1-s)q^2 + \tfrac{1}{4}\alpha q^4 - f_0 q\right]\right\} \quad (2)$$

where $\nu = 2\varsigma\varpi$ and N is normalization. For a prebuckled plate ($s < 1$) Eq. (2) has a single peak at near $q = 0$, and term $f_0 q$ brings about asymmetry into the otherwise symmetric quadratic and quartic terms. After buckling ($s > 1$), however, $f(q)$ becomes bimodal with the twin peaks at near $Q_\pm = \pm\sqrt{[\varpi^2(s-1)/\alpha]}$, the postbuckled plate displacements. Note that the asymmetry due to $f_0 q$ is manifested by the peaks at $Q_\pm$ being shifted slightly to the positive and that the Q_- peak gets lowered, whereas the Q_+ peak is raised.

In the previous study,[13] $f(q)$ is used to predict numerical displacement histograms of composite plates simulated by Vaicaitis[14] and Moorthy et al.[15] Here, we shall examine the more recent simulation of an aluminum plate carried out by Green and Killey.[16] In plate experiments,[17,18] one instead obtains strain histograms from the strain gauge output. It is, therefore, necessary to transform Eq. (2) into equilibrium strain distributions by the strain-displacement relationship[19]:

$$\varepsilon = C_0 + C_1 q + C_2 q^2 \quad (3)$$

where

$$C_0 = -\frac{(3 + 2\beta^2 + 3\beta^4)[t_0 + (t_0\delta_v/4)]}{9(1+\beta^2)(1+\mu)} + \frac{1}{72(1+\beta^2)^2}\left(t_0\delta_v(3 + 2\beta^2 + 3\beta^4)\left\{2\beta^2 \cos 2\pi x \cos 2\pi y - \frac{2(1+\beta^2)[-5 + (1+\mu)\cos 2\pi x]}{1+\mu}\right\}\right)$$

$$C_1 = -\tfrac{8}{3}\beta^2 \cos 2\pi x \sin^2(\pi y)$$

$$C_2 = -\frac{16\beta^2(-1+\beta^2\mu)\cos 2\pi x \cos 2\pi y}{9(1+\beta^2)^2} + \frac{8\beta^2(-1+4\beta^2\mu)\cos 4\pi x \cos 2\pi y}{9(1+4\beta^2)^2} + \frac{8\beta^2(-4+\beta^2\mu)\cos 2\pi x \cos 4\pi y}{9(4+\beta^2)} + \frac{2[4\mu\cos 2\pi x - \mu\cos 4\pi x + 8\beta^2\sin^4(\pi y)]}{9}$$

Because Eq. (3) is quadratic, there are two equilibrium strain distributions. In Ref. 13 we used only one of them to model experimental strain histograms and ignored the other. A main thrust of this paper is to investigate realizability of the strain distributions by a direct numerical simulation of Eq. (1). This will either justify the choice of strain distribution used in Ref. 13 or provide an alternate strain distribution as a realizable statistical solution of Eq. (1).

Displacement Histogram

We begin by examining the scaling property of the postbuckled distribution (2) for $s > 1$. For simplicity we restrict ourselves here to $f_0 = 0$, that is, zero temperature gradient across the plate thickness. We first transform Eq. (2) by $q = (2D/\alpha\nu)^{1/4} r$:

$$f(r) = N_1 \exp\left\{\tfrac{1}{2}(zr^2 - r^4)\right\} \quad (4)$$

where $z = \varpi^2(s-1)\sqrt{(2\nu/\alpha D)}$ and N_1 is another normalization. Because the mean of $f(q)$ is zero, the variance of $f(q)$ can be expressed by $\sigma^2 = (2D/\alpha\nu)^{1/2}\sigma_r^2$, where

$$\sigma_r^2 = \int_{-\infty}^{\infty} \exp\left\{\frac{1}{2}(zr^2 - r^4)\right\} r^2\,\mathrm{d}r \Big/ \int_{-\infty}^{\infty} \exp\left\{\frac{1}{2}(zr^2 - r^4)\right\}\mathrm{d}r$$

is the variance of $f(r)$. We have found $\sigma_r^2 \to z/2$ as z becomes large.[13] This means that, because Eq. (4) has peaks at $r = \pm\sqrt{(z/2)}$, it peaks out at $r = \pm\sigma_r$ as $z \to \infty$. By dropping the factor $(2D/\alpha\nu)^{1/4}$ we obtain a relationship $q/\sigma = r/\sigma_r$, from which the following observations are deduced: 1) $f(q/\sigma)$ is a symmetric distribution, 2) $f(q/\sigma)$ peaks out around $0.9 < |q/\sigma| < 1.1$, and 3) the actual range of $f(q/\sigma)$ is over $q/\sigma \approx \pm 2.6$, that is, $f(q/\sigma) \approx 0$ outside.

We previously have tested[13] the displacement histograms of Vaicaitis[14] and Moorthy et al.,[15] generated by the numerical simulation of composite plates. Apparently, the displacement histograms have the twin peaks at $q/\sigma \approx \pm 1$ (observation 2) and drop off to zero for $|q/\sigma| > 2.5$ (observation 3). However, the symmetry is somewhat lacking in their numerical histograms (observation 1), perhaps due to short simulation times. We must, however, point out that the choice of D is arbitrary. This is indeed necessary to reconcile between the single-mode Fokker–Planck distribution and direct numerical simulation of composite plates. Yet, we do not treat D as a completely arbitrary parameter. That is, once $D = 150$ is fixed for SPL = 130 dB, we adjust D by a factor 10 for 10 dB variation in the numerical simulations of Vaicaitis[14] and Moorthy et al.[15]

We now examine the recent numerical simulation of an aluminum plate by Green and Killey[16] using finite element codes. For the convenience of readers, we have reproduced here in Figs. 1–3 the three probability distribution functions (PDFs) taken from Figs. 12–14 of Ref. 16. Note that all PDFs correspond to $s = 1.71$ (i.e., the plate temperature 10°C above room temperature), but are under the three different SPL = 700 (150.9), 2000 (160), and 4000 Pa (166 dB).

At a low SPL = 700 Pa, displacement once negative remains negative, so that the excursion of displacement to positive is not observed in Fig. 1. However, when the SPL is raised to 2000 Pa, displacement can take on both the positive and negative values more or less equally, hence the PDF clusters around the positive and negative postbuckled positions, as shown in Fig. 2. This is a manifestation of random snap throughs. Now, at a higher SPL = 4000 Pa, the PDF of Fig. 3 appears bunching up around a single peak at zero displacement, rather than the twin peaks as in Fig. 2. Hence, Green and Killey[16] have concluded that a large acoustic load (SPL = 4000 Pa) obliterates the effect of thermal loading ($s = 1.71$), thus collapsing the twin peaks of displacement PDF. Such a conclusion, however, needs a qualifier on the respective roles of acoustic and thermal loads. To this end, let us first smooth out the jaggedness of Figs. 2 and 3 by consolidating PDF values over a window of width $\approx 0.1\sigma$, where σ is the standard deviation of displacement. We present in Figs. 4 and 5 such smoothed-out PDFs as the displacement histograms and superimpose on them Fokker–Planck distribution (4) computed with the parameter values of Table 1. Here, though arbitrary, we choose $D = 2$ for SPL = 160 dB (Fig. 4) and $D = 210^{0.6}$ for SPL = 166 dB (Fig. 5). The displacement histogram of Fig. 4 has two peaks in agreement with distribution (4). In contrast, Fig. 5 shows a large buildup at the zero displacement of histogram. This is at odds with the Fokker–Planck distribution. As we shall see, this is an artifact of numerical simulation.

For the numerical simulation under $f_0 = 0$, we rewrite Eq. (1) in terms of the explicit nondimensional variables and $\tau = t/\gamma$ and $g = \bar{g}(\tau)/g_{\mathrm{psi}}$, that is,

$$\ddot{q} + 2\varsigma\varpi\dot{q} + \varpi^2(1-s)q + \alpha q^3 = \bar{g}(\tau)/g_{\mathrm{psi}} \quad (5)$$

Now, the overdot denotes $\mathrm{d}/\mathrm{d}\tau$ and $\bar{g}$ is forcing expressed in pounds per square inch. As in common practice, the SPL will be expressed in decibels. For a given decibel level, we assume a constant power spectral density (PSD) over the frequency range of, for example,

Table 1 Parameters of Green and Killey[16]

Parameters	Numerical values
β, μ, ς, h	$\frac{350}{280}$, 0.33, 0.01, 1.2 mm
ϖ^2, α, ν	23.9, 85.4, 0.098
s(10°C)	$\frac{24}{14} = 1.71$

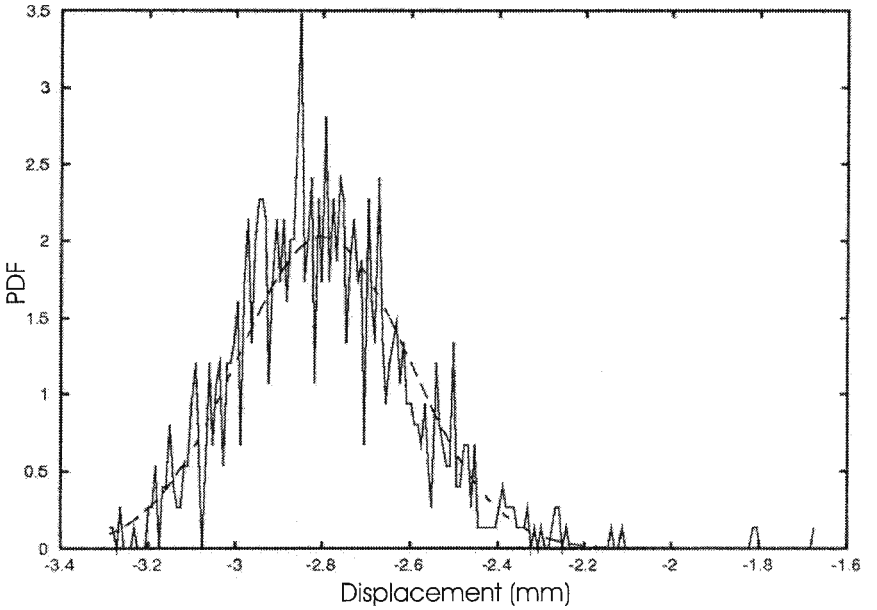

Fig. 1 Displacement PDF in Fig. 12 of Green and Killey[16] (thermal load = 10°C and SPL = 700 Pa).

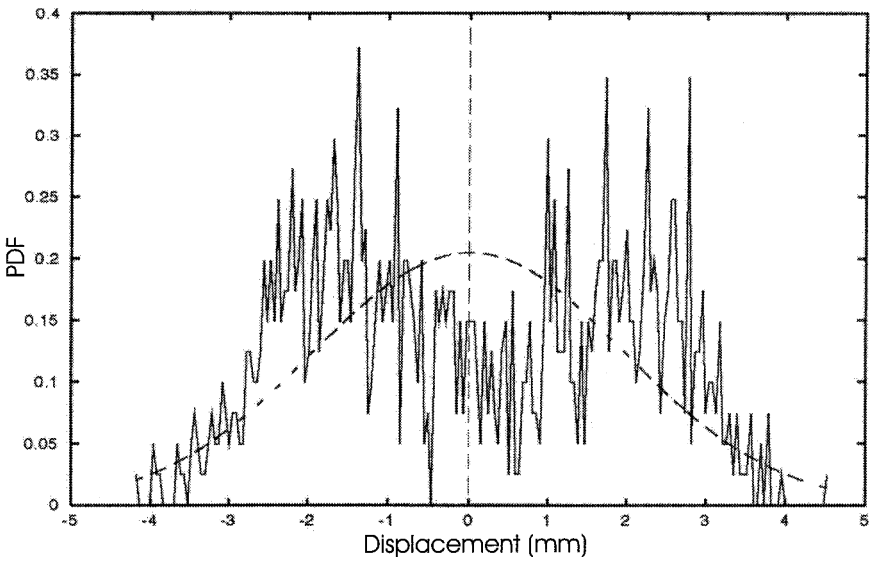

Fig. 2 Displacement PDF in Fig. 13 of Green and Killey[16] (thermal load = 10°C and SPL = 2000 Pa).

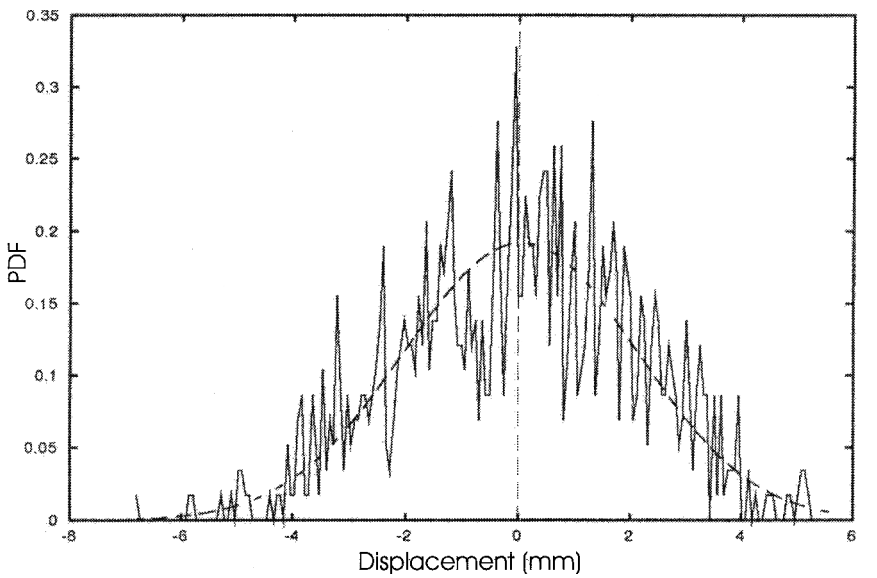

Fig. 3 Displacement PDF in Fig. 14 of Green and Killey[16] (thermal load = 10°C and SPL = 4000 Pa).

Table 2 SPL of numerical simulations under $s = 1.7$

Green and Killey's simulation,[16] dB	Present simulation, dB
150.9 (Fig. 1)	136 (Fig. 7)
160 (Fig. 2)	145 (Figs. 8 and 9)
166 (Fig. 3)	150 (Fig. 10)

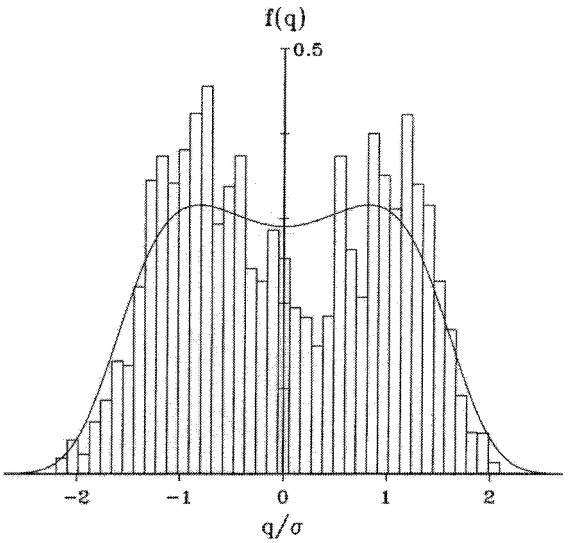

Fig. 4 Comparison of a smoothed-out histogram of Fig. 2 with Fokker–Planck distribution.

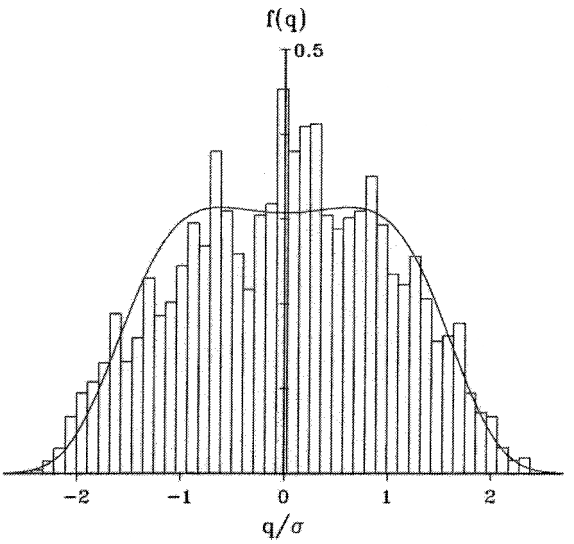

Fig. 5 Comparison of a smoothed-out histogram of Fig. 3 with Fokker–Planck distribution.

$f = (0, 2120$ Hz) in Fig. 6a, and construct a time series for $\bar{g}(\tau)$ by assigning random phases.[20,21] The amplitude of $\bar{g}(\tau)$ in Fig. 6b is parameterized by SPL, so that the mean squared $\bar{g}(\tau)$ has the same energy as contained in the constant PSD of Fig. 6a. Here, the number of frequency intervals, 1024, and time intervals, 4096, automatically specify the time integration interval, 0.0357, the detail of which is documented in Ref. 10. We simply point out that under $s = 1.7$ the values of SPL to match the typical displacement histograms of Figs. 1–3 are considerably smaller, as summarized in Table 2.

First, at SPL = 136 dB Fig. 7a shows that a trajectory with the initial negative q stays in the negative potential energy well, which is a part of the Hamiltonian surface drawn in Fig. 7b for better visualization. For the Hamiltonian of Eq. (5) we have $H = \frac{1}{2}p^2 - \frac{1}{2}\varpi^2(s-1)q^2 + \frac{1}{4}\alpha q^4$, where $p = \dot{q}$. Its surface is like pants with both legs tied up, and the depth of pant legs is given by

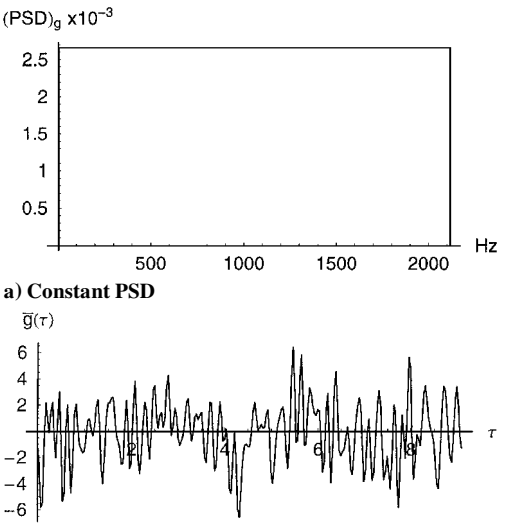

Fig. 6 Generation of white-noise forcing input of 145 dB.

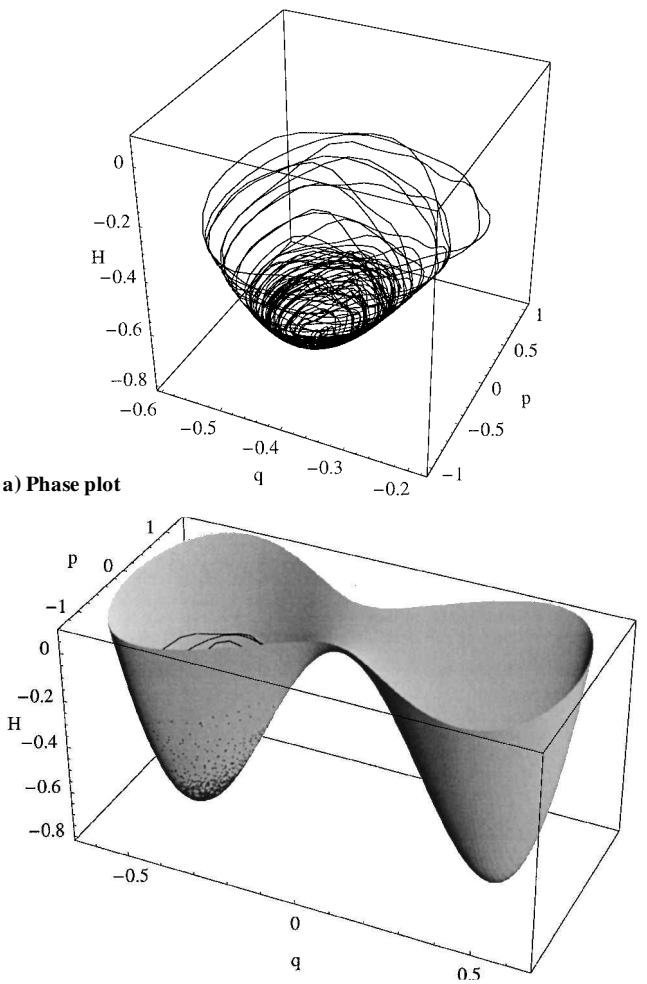

Fig. 7 Trajectory of Eq. (5) under SPL = 136 dB.

$-[\varpi^2(s-1)]^2/4\alpha$. In Fig. 7b the trajectory is trapped in the negative pants leg, and only a short rise above the separatrix is shown in Fig. 7b. Also, note that a continuous trajectory is not visible in Fig. 7b, because graphically the Hamiltonian surface hides the trajectory that lies behind it due to crude computation. In any event, it is clear that the trajectory of Fig. 7a will generate a displacement histogram that is confined entirely to the negative range of q. Next, for SPL = 145 dB the trajectory of Fig. 8a wanders randomly from

one potential energy well to the other because the forcing is large enough to overcome the potential barrier at $q = 0$. Graphically, the trajectory freely traverses both pants legs in Fig. 8b. This is a random snap through under random excitations, in contrast to the chaotic snap through that occurs under a deterministic forcing. Note that the pants legs in Figs. 7b and 8b are of the same length, corresponding to the same thermal loading $s = 1.7$. The only difference is that Fig. 8b has a higher rise above the separatrix than Fig. 7b, reflecting the difference in the acoustic loads.

Figure 9 shows a displacement histogram constructed from the trajectory of Fig. 8, which is compared with Fokker–Planck distribution (4). Here, because D is known from the generation of $\bar{g}(\tau)$, there is no arbitrariness in distribution (4). Just as in Fig. 2, the displacement histogram of Fig. 9 has much sharper peaks than the Fokker–Planck distribution. This clearly is a manifestation of snap-through dynamics, whereas the Fokker–Planck distribution is purely a statistical description of displacements that are distributed randomly according to the potential energy well. Lastly, we present in Fig. 10 the displacement histogram of trajectory of Eq. (5) under SPL = 150 dB. There develops a broad plateau over $-1 < q/\sigma < 1$, thereby indicating the dominance of acoustic load over thermal loading. Nonetheless, unlike in Fig. 3, the displacement histogram of Fig. 10 does not build up at $q \approx 0$. This is because under $s = 1.7$ the Hamiltonian surface is still like the pair of pants, even though the pants legs are much shorter than the rise above the separatrix at SPL = 150 dB.

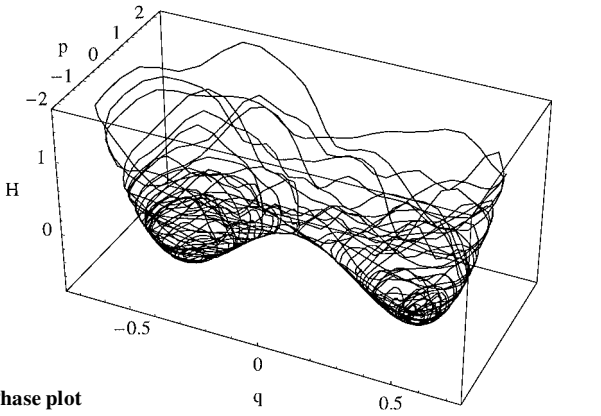

a) Phase plot

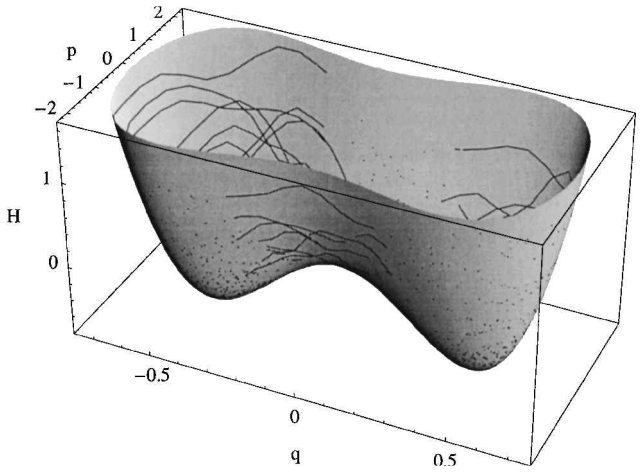

b) Phase plot on the Hamiltonian surface

Fig. 8 Trajectory of Eq. (5) under SPL = 145 dB.

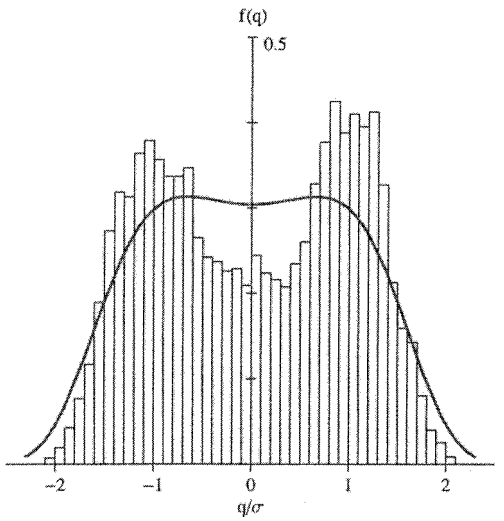

Fig. 9 Comparison of the displacement histogram under SPL = 145 dB with Fokker–Planck distribution.

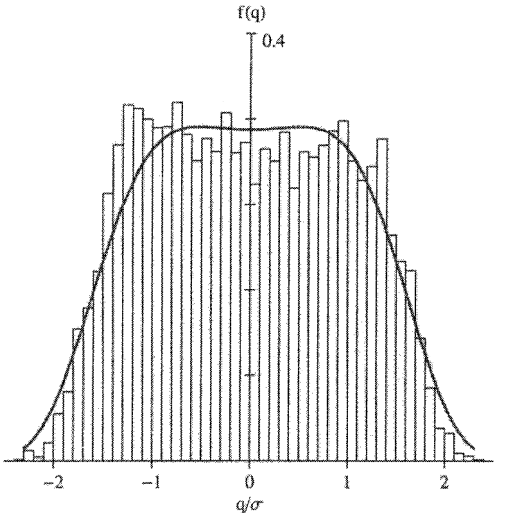

Fig. 10 Comparison of the displacement histogram under SPL = 150 dB with Fokker–Planck distribution.

Strain Histogram

Displacement is the first thing to compute in numerical simulations, and we have shown that displacement histograms obey the pertinent features of distribution (4) as delineated by observations 1–3. This is because the Fokker–Planck distribution has proven a realizable statistical solution of Eq. (5). In plate experiments,[17,18] however, one obtains strain time series, and hence histograms, from a strain gauge mounted on thermally buckled plates in random vibration. It is therefore desirous to derive equilibrium strain distribution $f(\varepsilon)$ from the Fokker–Planck distribution $f(q)$ through transformation[19] by the strain-displacement relationship. Then, inverting Eq. (3) for q by the quadratic root formula, we have

$$q_{\pm} = \left[-C_1 \pm \sqrt{C_1^2 - 4C_2(C_0 - \varepsilon)}\right] \Big/ 2C_2 \tag{6}$$

For a strain gauge mounted at the midpoint along a longer plate edge,[17,18] we accordingly evaluate constant C_0, C_1, and C_2 in Eq. (3) at $x = 0$ and $y = \frac{1}{2}$. Then, inserting $q_{\pm}$ into distribution (2), we have two equilibrium strain distributions, $f_+(\varepsilon)$ and $f_-(\varepsilon)$, for q_+ and q_-, respectively. However, we do not know a priori which or both of $f_+(\varepsilon)$ and $f_-(\varepsilon)$ are realizable in numerical simulation. In any event, for the parameter values of Table 1, we present in Fig. 11 the surface plots of $f_+(\varepsilon)$ and $f_-(\varepsilon)$ over the range of $D = (0.1, 3)$ under $f_0 = 0$. As already noted,[13] both $f_{\pm}(\varepsilon)$ have the negative cutoff $\varepsilon_t = C_0 - C_1^2/4C_2 \approx -2$, although there is no upper strain limit for $\varepsilon \to +\infty$. Here, ε_t corresponds to the radicand of Eq. (6) being zero. The left-hand side faces of the three-dimensional box frame are positioned at $\varepsilon = \varepsilon_t$ in Fig. 11, hence, the negative strain cutoff for $f_{\pm}(\varepsilon)$. Though not evident in Fig. 11 due to arbitrary scaling, note that $f_+(\varepsilon_t) = f_-(\varepsilon_t)$ as shown in Fig. 12.

Because $f_+(\varepsilon) \approx 0$ as $D \to 0$ (Fig. 11a), we dropped it altogether and considered only $f_-(\varepsilon)$ for small D in our previous work.[13]

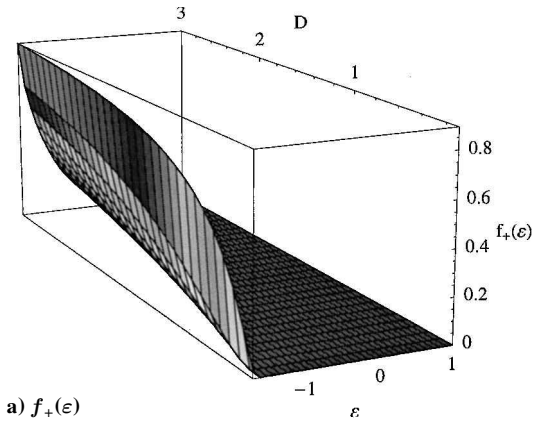

a) $f_+(\varepsilon)$

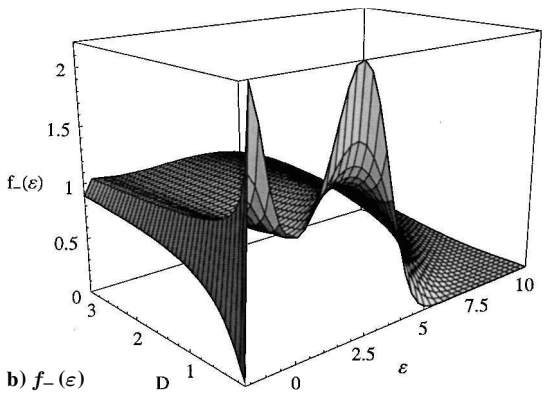

b) $f_-(\varepsilon)$

Fig. 11 Equilibrium strain distribution over the forcing range D = (0.1, 3).

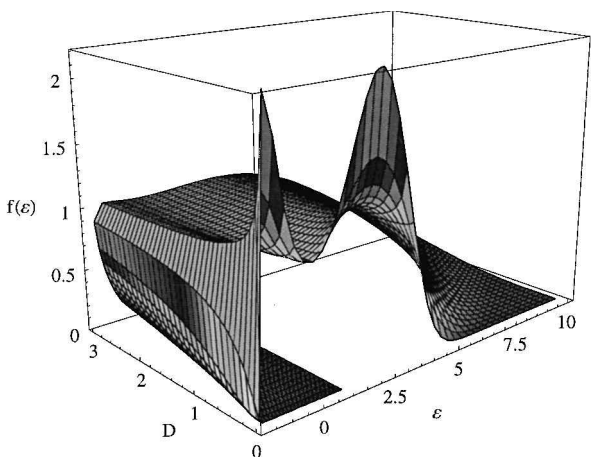

Fig. 12 Composite strain distribution of $f_+(\varepsilon)$ and $f_-(\varepsilon)$.

This has been further motivated by the ability of $f_-(\varepsilon)$ to model experimental strain histograms, as typified by the strain histogram of Ng[17] in Fig. 13. Namely, Fig. 14 shows that the strain peak heights of $f_-(\varepsilon)$ become unequal when a temperature gradient of $\delta_g = 0.3$ is imposed across the plate thickness. Therefore, we can capture by $f_-(\varepsilon)$ the following features of strain histograms: 4) $f_-(\varepsilon)$ is asymmetric with a negative strain cutoff, 5) the negative strain peak is sharper than the positive strain peak, and 6) a positive temperature gradient ($\delta_g > 0$) raises the negative strain peak and lowers the positive strain peak.

Observations 4–6 are confirmed qualitatively by the experimental strain histograms.[17,18] Yet, there are a few ambiguities. First, it was necessary to shift $f_-(\varepsilon)$, by $+0.3\sigma_\varepsilon$, where σ_ε is the standard deviation of strain, to better fit the experimental strain peaks in Fig. 13. Second, a temperature gradient across the plate thickness

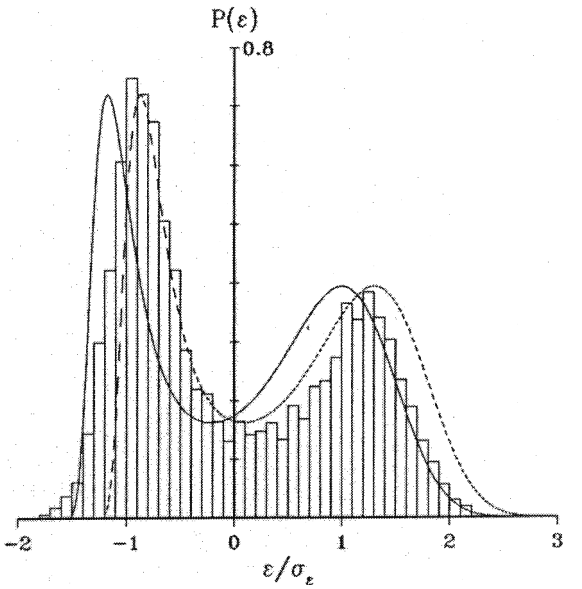

Fig. 13 Comparison of the experimental strain histogram of Ng[17] with $f_-(\varepsilon)$; ——, no shifting, and – – –, shifted by $+0.3\sigma_\varepsilon$.

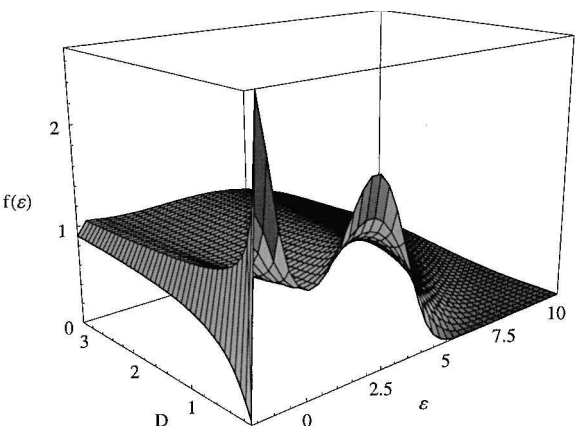

Fig. 14 Unequal strain peak heights due to temperature gradient (δ_g = 0.3) across the plate thickness.

is now needed to bring about the unequal peak heights of strain histograms. To resolve these ambiguities, we ask, to what strain distribution will numerical simulation of Eq. (5) lead under $f_0 = 0$? This is the question of realizability of $f_\pm(\varepsilon)$.

To this end, we simulate Eq. (5) to generate a displacement time series under $f_0 = 0$, as before, but now we transform it to a strain time series by strain-displacement relation (3). We are, however, surprised to find that the numerical strain histogram in Fig. 15 is more asymmetrically skewed than the experimental histogram of Fig. 13, but without the help of the temperature gradient. This is a clear indication that the numerical simulation of Eq. (5) does not simply lead to the equilibrium statistical state of $f_-(\varepsilon)$. Nonetheless, we can bound the numerical strain histogram of Fig. 15 by a linear combination $\phi f_+(\varepsilon) + (1-\phi) f_-(\varepsilon)$ with the choice of $\phi = 0.25$. That is, the actual strain distribution lies somewhere in between $f_+(\varepsilon)$ and $f_-(\varepsilon)$. This, therefore, alters the role that temperature gradient plays in strain histograms; the unequal strain peaks are no longer hinged on a temperature gradient across the plate thickness, as stipulated in observation 6. To exhibit the role of temperature gradient, it is indeed desirous to design a plate experiment so that one can switch on or off a temperature gradient by heating a plate only on one side or both sides. Although K. D. Murphy, as related in a private communication in August 1999, attempted a plate experiment of this sort, no conclusive evidence has yet been obtained to validate the role of temperature gradient across the plate thickness.

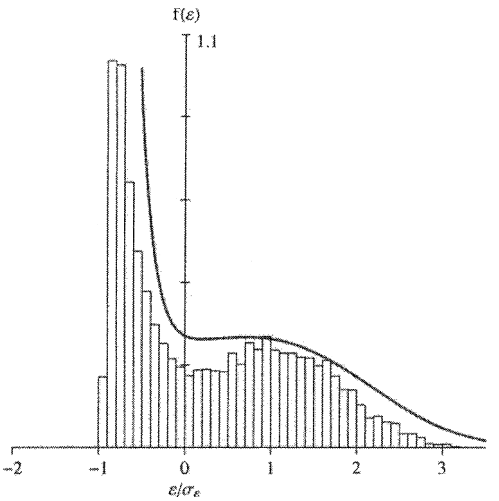

Fig. 15 Strain histogram from the simulation of Eq. (5) under SPL = 150 dB; ——, $0.25f_+(\varepsilon) + 0.75f_-(\varepsilon)$.

Conclusions

In the previous work, we used the single-mode Fokker–Planck distribution (2) to predict displacement histograms of the numerical simulations[14,15] and strain histograms of the plate experiments.[17,18] In this paper, we investigate realizability of the equilibrium displacement and strain distributions directly from the numerical simulation of single-mode Eq. (5) of motion. First, we find that distribution (4) is realizable as a statistical solution of Eq. (5) and, thus, provides a theoretical framework to assess consistency of the recent numerical simulation of Green and Killey.[16] Second, we obtain two equilibrium strain distributions from the transformation of Fokker–Planck distribution via the quadratic strain-displacement relationship. It is shown that numerical simulation of Eq. (5) does not lead to either one of the equilibrium strain distributions as a stationary statistical state, but to a strain distribution that can be modeled by a linear combination of the two. The upshot is that the unequal strain peaks in histograms are not necessarily due to a temperature gradient across the plate thickness, as previously proposed.[13]

Acknowledgment

This work was supported in part by the Air Force Office of Scientific Research New World Vista.

References

[1]Lee, J., "Large Amplitude Plate Vibration in an Elevated Thermal Environment," *Applied Mechanics Reviews*, Vol. 46, No. 2, 1993, pp. S242–254.

[2]Jacobson, M. J., and Maurer, O. F., "Oil Canning of Metallic Panels in Thermal-Acoustic Environment," AIAA Paper 74-982, Aug. 1974.

[3]Jacobson, M. J., "Sonic Fatigue of Advanced Composite Panels in Thermal Environments," *Journal of Aircraft*, Vol. 20, No. 3, 1983, pp. 282–288.

[4]Bisplinghoff, R. L., and Pian, T. H. H., "On the Vibrations of Thermally Buckled Bars and Plates," TR 25-22, Aeroelastic and Structures Research Lab., MIT, 1957.

[5]Tseng, W.-Y., "Nonlinear Vibration of Straight and Buckled Beams Under Harmonic Excitation," AFOSR 69-2157TR, Air Force Office of Scientific Research, Arlington, VA, Nov. 1969.

[6]Seide, P., and Adami, C., "Dynamic Stability of Beams in a Combined Thermal-Acoustic Environment," Flight Dynamics Lab., Air Force Wright Aeronautical Labs., AFWAL-TR-83-3072, Wright–Patterson AFB, OH, Oct. 1983.

[7]Ng, C. F., "Nonlinear and Snap-Through Responses of Curved Panels to Intense Acoustic Excitation," *Journal of Aircraft*, Vol. 26, No. 3, 1989, pp. 281–288.

[8]Ng, C. F., and Clevenson, S. A., "High-Intensity Acoustic Tests of a Thermally Stressed Plate," *Journal of Aircraft*, Vol. 28, No. 4, 1991, pp. 275–281.

[9]Ng, C. F., and Wentz, K. R., "The Prediction and Measurement of Thermoacoustic Response of Plate Structures," AIAA Paper 90-0988, April 1990.

[10]Lee, J., and Wentz, K. R., "Strain Power Spectra of a Thermally Buckled Plate in Random Vibration," *Proceedings of the 6th International Conference on Recent Advances in Structural Dynamics*, edited by N. S. Ferguson, H. F. Wolfe, and C. Mei, Vol. 2, Univ. of Southampton, Southampton, UK, 1997, pp. 903–917.

[11]Caughey, T. K., "Derivation and Application of the Fokker–Planck Equation to Discrete Nonlinear Dynamical Systems Subjected to White Random Excitations," *Journal of the Acoustical Society of America*, Vol. 35, No. 11, 1963, pp. 1683–1692.

[12]Andronov, A. A., Vitt, A. A., and Pontryagin, L. S., "On the Statistical Investigation of Dynamical Systems," *Journal of Experimental and Theoretical Physics* (Russian ZETP), Vol. 3, No. 3, 1933, pp. 165–180; also *A.A. Andronov Selected Works*, Academy of Sciences, USSR, 1956, pp. 142–160.

[13]Lee, J., "Random Vibration of Thermally Buckled Plates: II Nonzero Temperature Gradient Across the Plate Thickness," *Applied Mechanics Reviews*, Vol. 50, No. 11, 1997, pp. S105–116.

[14]Vaicaitis, R., "Response of Composite Panels Under Severe Thermo-Acoustic Loads," Aerospace Structures Information and Analysis Center, TR-94-05, Wright–Patterson AFB, OH, Feb. 1994.

[15]Moorthy, J., Mei, C., and Shirahatti, U., "Numerical Simulation of Acoustically Induced Nonlinear Variations of a Plate with Temperature Gradient," AIAA Paper 95-1378, April 1995.

[16]Green, P. D., and Killey, A., "Time Domain Dynamic Finite Element Modelling in Acoustic Fatigue Design," *Proceedings of the 6th International Conference on Recent Advances in Structural Dynamics*, edited by N. S. Ferguson, H. F. Wolfe, and C. Mei, Vol. 2, Univ. of Southampton, Southampton, U.K., 1997, pp. 1007–1025.

[17]Ng, C. F., "Theoretical and Experimental Studies of Thermal-Acoustic Response of Aircraft Structures," *Proceedings of ASIA-PACIFIC Vibration Conference*, 1993, pp. 1928–1933.

[18]Istenes, R. R., Jr., Rizzi, S. A., and Wolfe, H. F., "Experimental Nonlinear Random Vibration Results of Thermally Buckled Composite Panels," AIAA Paper 95-1345, April 1995.

[19]Stratonovich, P. L., *Topics in the Theory of Random Noise*, Vol. 1, Gordon and Breach, New York, 1963, p. 206, Chap. 8.

[20]Shinozuka, M., and Jan, C. M., "Digital Simulation of Random Process and its Applications," *Journal of Sound and Vibration*, Vol. 25, No. 1, 1972, pp. 111–128.

[21]Vaicaitis, R., "Nonlinear Response and Sonic Fatigue of National Aerospace Plane Surface Panels," *Journal of Aircraft*, Vol. 31, No. 1, 1994, pp. 10–18.